Room-Temperature Implementation of the Quantum Streaming Algorithm in a Single Solid-State Spin Qubit

Fei-Fei Yan,[1,2,§] Zhen-Peng Xu,[3,§] Qiang Li,[1,2] Jun-Feng Wang,[1,2] Ji-Yang Zhou,[1,2] Wu-Xi Lin,[1,2] Jin-Shi Xu,[1,2,*] Yuyi Wang,[4,†] Chuan-Feng Li,[1,2,‡] and Guang-Can Guo[1,2]

[1] *CAS Key Laboratory of Quantum Information, University of Science and Technology of China, Hefei 230026, People's Republic of China*

[2] *CAS centre for Excellence in Quantum Information and Quantum Physics, University of Science and Technology of China, Hefei, Anhui 230026, People's Republic of China*

[3] *Naturwissenschaftlich-Technische Fakultät, Universität Siegen, Walter-Flex-Straße 3, Siegen 57068, Germany*

[4] *Disco Group, ETH Zurich, Zurich 8092, Switzerland*

(Received 24 August 2020; revised 26 July 2021; accepted 4 August 2021; published 16 August 2021)

Great challenges are encountered when solving problems based on continuously generated data streams due to the online data input fashion and limited memory space. Quantum properties are helpful in dealing with stream data. In this work, we design and experimentally implement a quantum streaming algorithm (QSA) with various lengths of input data in a single-defect spin system in silicon carbide at room temperature. We explore the schemes with trusted advice on the output results during the algorithm execution. Quite contrary to the classical case, outdated advice is still useful in the quantum case, as revealed by a proper performance function. Our work demonstrates the advantage of the QSA, which would be useful for investigating complex online problems. The room-temperature solid-state spin platform based on such a technological material opens the door for scalable quantum-information processing.

DOI: 10.1103/PhysRevApplied.16.024027

I. INTRODUCTION

Streaming algorithms deal with data streams, in which the input is revealed as a sequence of items. Algorithms of this type are becoming increasingly relevant nowadays because data are generated over time in many applications, such as videos produced by traffic monitoring cameras, and one cannot collect all these data at once. The size of the generated data increases, while the storage-space size remains constant in a reasonable period of time; hence, one cannot store all the generated data, and some information is inevitably lost. Two main challenges are encountered when designing streaming algorithms. First, the input comes in an online fashion, and online algorithms usually can only make suboptimal decisions (e.g., online matching [1,2], online k-server problem [3,4], and ski-rental problem [5,6]). Second, streaming algorithms can only use a limited memory; hence, in this situation, even a very simple question related to the whole input is hard to answer accurately [7]. For the first challenge, the difficulty of online problems and the performance of online algorithms are evaluated by competitive ratio [8] and advice complexity [9,10]. For the second challenge, we often analyze the accuracy that streaming algorithms can achieve given a certain amount of memory.

Some efficient quantum algorithms have also been proposed, including Shor's algorithm for factoring [11] and Grover's algorithm for searching [12]. Both provide a high speedup over their classical counterparts. Moreover, quantum properties are helpful for online and streaming computation, in which the exponential separation of the quantum and classical online space complexity has been found [13]. Theoretical developments further support the possibility to design advanced quantum streaming algorithms (QSAs). More classical bits are needed to simulate a randomized quantum process of a given number of qubits or qutrits [14,15], and any number of classical bits cannot simulate even a deterministic quantum process of a qubit in principle [16]. A QSA with only one qubit was recently proposed and found to perform better than any classical ones for both cases with or without advice in a sublogarithmic space (memory) [3].

In this work, we experimentally implement a QSA with a single-defect spin in silicon carbide (SiC) at room temperature, which is a very promising platform for scalable quantum-information processing [17]. Defect spins can be polarized, read out by laser beams, and manipulated by a

*jsxu@ustc.edu.cn
†yuwang@ethz.ch
‡cfli@ustc.edu.cn
§These authors contributed equally to this work.

microwave at even room temperature. The random input data stream is translated as the spin rotations by implementing well-designed microwave pulses. Successful output probabilities are detected to be larger than those of the classical algorithm with a single bit. Both cases with and without advice providing the corresponding output information in the quantum algorithm are demonstrated. Our results would be useful for investigating quantum online algorithms. The verified efficient QSA in such a quantum processor based on the technological material SiC would pave the way for future scalable quantum simulation and computation.

II. QUANTUM STREAM ALGORITHM

One of the representative examples in dealing with streaming data is the problem of (n,p,k,r,w) parity for number of hats (PNHs) [3]. For an input stream of binary strings $\{X_1,\ldots,X_p\}$, the number of 1's in X_i, which is denoted as $\text{no.}_1(X_i)$, is assumed to be in the form of $\text{no.}_1(X_i) = v(X_i)\times 2^k$, where $v(X_i), k \in \mathbb{Z}$. The stream length of X_i is denoted as m_i, and the total length is denoted as n, that is, $n = \sum_{i=1}^{p} m_i$. During the algorithm implementation, the binary value of y_j is the measurement result before each stream X_j. Another value z_j depends on j and the future sequence. Mathematically, $z_j = \bigoplus_{i=j}^{p} Partial\text{MOD}_{m_i}^{k}(X_i)$, where $Partial\text{MOD}_{m_i}^{k}(X_i) = v(X_i) \mod 2$. Generally, the algorithm can take advantage of extra advice about z_j at a certain stage, thus the performance can be enhanced. The algorithm performance is judged by a function related to the accuracy of y_j's to z_j's, which can be defined from the viewpoint of resource cost as cost $= r$ if $y_i = z_i$, and cost $= w$ otherwise [3]. Usually, $r < w$. Characterized by this function, a quantum algorithm always has an advantage over the classical one, regardless of the presence or absence of an advice. In the classical algorithm, the advice about z_1 is not useful anymore if it is received after the y_1 output. However, quite contrary to the classical case, the outdated advice is still helpful in the quantum case, as revealed by our adapted quantum algorithm with a proper performance function. The average score of the performance function is defined as

$$\overline{S} = \sum_{j=1}^{2^p} P_j\,(2^{\sum_{i=1}^{p}\delta(y_i,z_i)} - 1), \tag{1}$$

where, $\delta(y_i,z_i) = 1$ when $y_i = z_i$ and $\delta(y_i,z_i) = 0$ when $y_i \neq z_i$. The expression of $2^{\sum_{i=1}^{p}\delta(y_i,z_i)} - 1$ represents the score of each binary output sequence of $\{y_1,\ldots,y_p\}$ with P_j representing the corresponding probability.

We now consider the quantum stream algorithm shown in Fig. 1(a) with three input binary data streams X_1, X_2, and X_3. The initial state of the qubit Q_1 is prepared as $(|0\rangle + |1\rangle)/\sqrt{2}$, with $|0\rangle$ and $|1\rangle$ as the two energy levels. During the algorithm, the Pauli σ_z operator measurement (M) is performed at the initial stage and after the data streams X_1 and X_2, where y_1, y_2, and y_3 are the corresponding results. We consider a simple case when a trusted adviser provides the information of whether $y_1 = z_1$ (advice) at a different algorithm stage [dotted arrow in Fig. 1(a)], in which corresponding actions can be taken to increase the average score of the performance function. For example, when the advice is provided before the first measurement, we can then directly rotate the initial state to $|z_1\rangle$ and then perform the measurement. If the advice is provided after the first measurement, no action is taken if $y_1 = z_1$; otherwise, we would perform a NOT gate on the state before the next measurement.

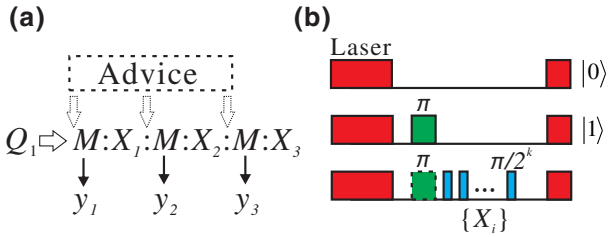

FIG. 1. Quantum stream algorithm. (a) Logic diagram of the stream algorithm. Q_1 represents a single qubit; M means the measurement on the qubit state; and y_i denotes the corresponding results. $X_i \in \{0,1\}^{m_i}$ are the input binary data stream. Advice is applied at different algorithm stages to correct the output results. (b) Pulse sequences. The red strips represent the laser duration with the first and last ones used to initialize and read out the corresponding states; the green strip represents the π operation for state flipping between $|0\rangle$ and $|1\rangle$; the blue strips represent blue microwave pulses to implement the X_i operation with $\alpha = \pi/2^k$ rotation corresponding to input 1 and an idle operation corresponding to input 0.

To realize the algorithm, the information carrier can be encoded as an optically addressable spin qubit, in which the spin state can be optically initialized, read out, and manipulated by microwaves. Figure 1(b) shows the pulse sequences. The red strips represent the laser pulses used to initialize and read out the spin states. The green and blue strips represent the microwave pulses to rotate the spin states. The first two sets of sequences determine the normalized photon counts ($n_{|0\rangle}$ and $n_{|1\rangle}$) when the states are in $|0\rangle$ and $|1\rangle$. When reading the binary data stream, an $\alpha = \pi/2^k$ rotation is implemented when reading 1, while no action is taken when reading 0.

III. EXPERIMENTAL RESULTS

The defect spins in SiC have attracted great interest due to their excellent properties [18–20]. In this work, the information carrier is represented by a single divacancy spin, called PL5 [21]. The sample used is a SiC

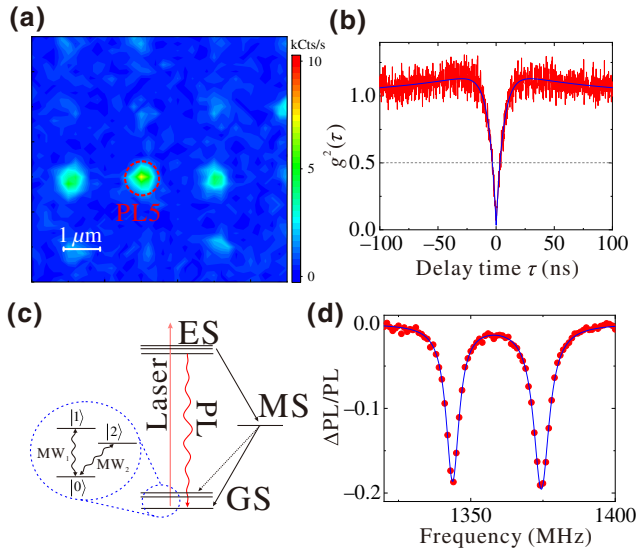

FIG. 2. Single spin defect in 4H-SiC. (a) Confocal scan image of the SiC epitaxy sample implanted by carbon ions. The single spin defect, called PL5, is denoted in the red dashed circle. The white scale bar is 1 μm. (b) Correlation function $g^2(\tau)$ measurement of the single PL5 defect shown in (a). The blue line is the fitting. The zero delayed value of $g^2(0)$ is fitted to be approximately 0.03, which is greatly less than 0.5 and indicates the single defect. (c) Proposed energy-level diagram of PL5. GS, ES, and MS represent the ground state, excited state, and metastable state, respectively. The PL photons are collected. The GS spin is split as a three-level system, with $|0\rangle$, $|1\rangle$, and $|2\rangle$ as the corresponding states. MW_1 and MW_2 show the resonant microwave frequency between $|0\rangle \leftrightarrow |1\rangle$ and $|0\rangle \leftrightarrow |2\rangle$. (d) Room-temperature optical detected magnetic resonance (ODMR) spectrum for the PL5 spin with zero external magnetic fields. The red dots are the experimental data. The blue line is the Lorentz fit showing that the resonance frequencies are 1374.4 MHz (MW_1) and 1343.7 MHz (MW_2).

high-purity epitaxy layer, which is implanted by carbon ions and subsequently annealed to generate single-defect arrays [22,23]. A 920-nm laser is used to excite the defect through a home-built confocal imaging system. The photoluminescence is collected by the same setup after a 1000-nm long-pass filter and detected by a superconducting single-photon detector. Figure 2(a) shows a typical scanning image. The white scale bar is 1 μm. The point denoted by the red circle is a single PL5 defect verified through the correlation function $g^2(\tau)$ measurement shown in Fig. 2(b). The zero delay time $[g^2(0)]$ is fitted to be 0.03, which is greatly smaller than 0.5 and indicates a single emitter. Figure 2(c) depicts the proposed energy-level structure. The ground state with the spin $S = 1$ ($|0\rangle$, $|1\rangle$, and $|2\rangle$ represent the three separated energy levels) can be manipulated by microwave pulses. MW_1 and MW_2 represent the resonant microwave frequencies between states $|0\rangle \leftrightarrow |1\rangle$ and $|0\rangle \leftrightarrow |2\rangle$, respectively. Microwaves are applied through a 20-μm copper wire mounted on the sample surface. Figure 2(d) shows the corresponding room-temperature ODMR spectrum with the two frequencies deduced as 1374.4 and 1343.7 MHz. The zero-field parameters $|D|$ and $|E|$ are 1359.05 and 15.35 MHz, respectively, for the basal-axis PL5 defect [21].

In our experiment, Q_1 is encoded into two spin levels $|0\rangle$ and $|1\rangle$ of PL5. The spin state after the algorithm operation can be read out with the photon counts denoted as n_{X_i}. The probability that the state on $|1\rangle$ is read as $P_{|1\rangle} = (n_{|0\rangle} - n_{X_i})/(n_{|0\rangle} - n_{|1\rangle})$. Theoretically, the microwave pulses can always be designed to let the final spin state be $|0\rangle$ ($|1\rangle$) with the corresponding probabilities of $P_{|1\rangle} = 0$ ($P_{|1\rangle} = 1$). However, the detected probability would be affected by the experimental errors and the environmental noise, and $0 < P_{|1\rangle} < 1$ would be obtained in practice.

To experimentally run the QSA, we must determine the applied microwave duration time T_α with the operation of $\alpha = \pi/2^k$ on the spin state when the input data stream meets 1. We then measure the spin Rabi oscillation shown in Fig. 3(a). The red dots in the figure depict the experimental data, while the blue solid line denotes the theoretical fitting. The π pulse duration is 0.704 μs, and the decay time is $T_2' = 9.5 \pm 0.6$ μs. When the input data stream meets 0, we apply an idle pulse with 10-ns duration time, but no microwave. The coupling with the environmental noise leads to a free induction decay for the spin qubit, which is measured and shown in Fig. 3(b). From the fitting, we deduce the dephase time T_2^* as 1.42 ± 0.04 μs. We further explore the state rotation during the experiment for two randomly chosen binary data streams X_1 and X_2 [Fig. 3(c)]. The length of each data stream is 9. The rotation angle is $\pi/4$ when the input binary data stream reading 1 and is represented by the green strip. We only considered the case with the measurement result of $y_1 = 1$ herein to clearly show the state evolution during the algorithm implementation. After the stream data X_1 operation, $P_{|1\rangle} = 0.91$, which is greatly larger than 0.5. For X_2, the final result of $P_{|1\rangle}$ is 0.12, which is smaller than 0.5.

Three kinds of gates are implemented in the experiment, that is, the NOT gate (flipping between $|0\rangle$ and $|1\rangle$), 0 gate (idle operation), and 1 gate (rotating the spin with an angle of $\pi/2^k$). The gate fidelities can be estimated by considering the environmental noises (see Appendix A for more details). In our experiment, the fidelity of the NOT gate is estimated as $F_{\mathrm{NOT}} = 0.928 \pm 0.017$, with $t_\pi = 0.704 \pm 0.001$ μs, while those of the 0 gate and 1 gate are $\overline{F}_0 = 0.999\,98 \pm 0.000\,01$ and $\overline{F}_1 = 0.9889 \pm 0.0008$ with $k = 2$, respectively.

We further implement the quantum stream algorithm with $k = 4$ and compare the experimental results with the predictions using a single classical bit [Fig. 4(a)]. Three sets of randomly selected different binary data streams $\{X_1, X_2, X_3\}$ are used, denoted as $S.1$ (red squares), $S.2$ (purple up triangles), and $S.3$ (blown down triangles),

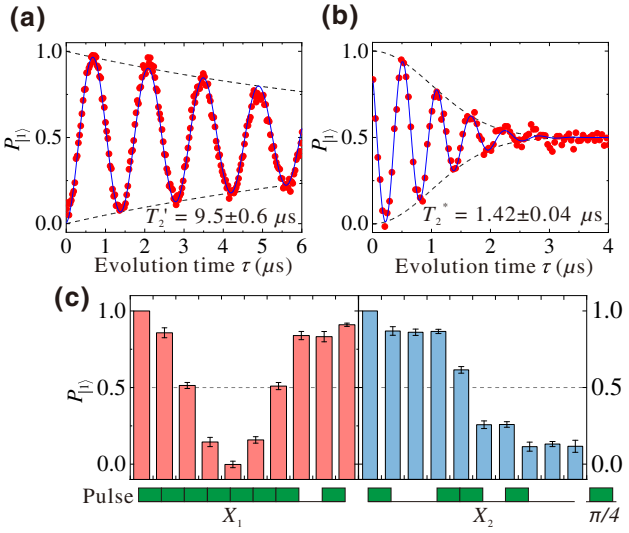

FIG. 3. Spin properties and state evolution. (a) Rabi oscillation of the single PL5 spin at zero magnetic fields. The population of state $|1\rangle$ oscillates and decays with the increase of the evolution time. The decay time is $T_2' = 9.5 \pm 0.6\ \mu$s. The oscillation period is $T_{2\pi} = 1.408 \pm 0.002\ \mu$s. The red dots depict the experimental results. The blue line denotes the fitting. The two dashed lines represent the decay curves. (b) Ramsey oscillation of the spin with a detuning frequency $\delta f = 1.7$ MHz at zero magnetic fields. The biexponential decay fitting gives the free induction decay time $T_2^* = 1.42 \pm 0.04\ \mu$s. The red dots illustrate the experimental results. The blue line depicts the fitting. The two dashed lines represent the decay curves. (c) State evolution during the algorithm implementation. X_1 and X_2 are the two randomly chosen binary data stream for $k = 2$. If the input data stream meets 1, the spin is rotated by a $\pi/4$ microwave pulse (green strip). If the input data stream meets 0, an idle pulse with the 10-ns duration time of is applied. The projection probabilities of state $|1\rangle$ are shown as the red and blue columns for the input binary data streams X_1 and X_2, respectively.

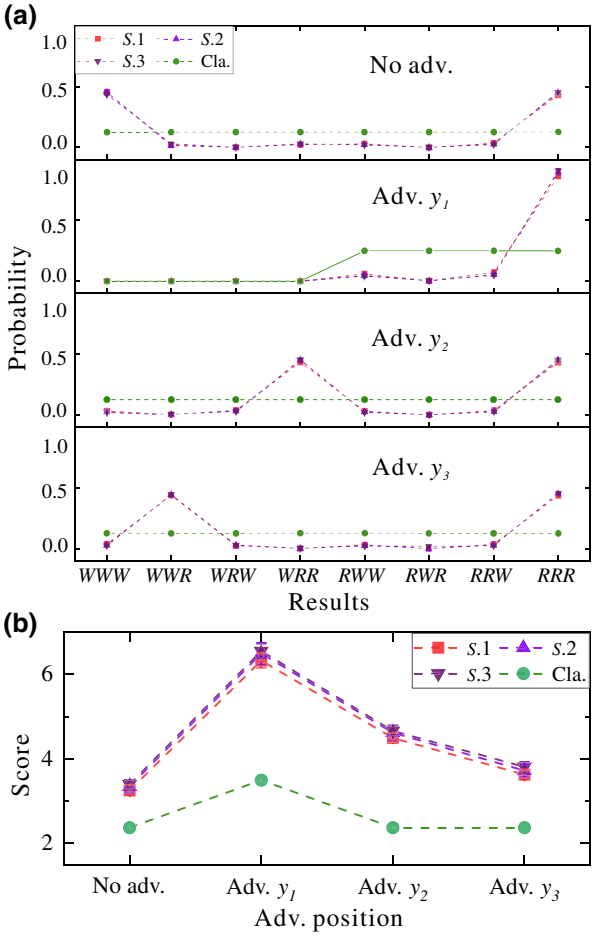

FIG. 4. Experimental results for $k = 4$. (a) Experimental results for three different stream data settings $\{X_1, X_2, X_3\}$ represented by $S.1$ (red squares), $S.2$ (purple up triangles), and $S.3$ (blown down triangles), respectively. The X_i length is set to 40, and k is equal to 4. The classical prediction results (Cla., green dots) with a single classical bit are provided for comparison. No adv. represents the case with no advice in the process. Adv. y_1, Adv. y_2, and Adv. y_3 represent the cases with advice before the y_1, y_2, and y_3 measurement, respectively. The correct output $y_i = z_i$ is defined as "R" and "W" otherwise. The results of $y_1y_2y_3$ vary from "WWW" to "RRR." (b) Average scores with advice at different stages. The algorithm with a single qubit performs better than that with a single classical bit for all cases.

respectively. The results of the classical case (Cla.) are denoted by the green dots. The length of each data stream X_i is set to 40. Table I in Appendix B presents the detailed binary data stream. For the quantum case with a single qubit, we start with the initial superposition state $(|0\rangle + |1\rangle)/\sqrt{2}$. The probability of acquiring the right (R) result with $y_1 = z_1$ is 50%. The corresponding wrong (W) probability is also 50%. Both $|0\rangle$ and $|1\rangle$ states are prepared and evolved according to data stream X_1. The right probability with $y_2 = z_2$ and the corresponding wrong probability would be obtained in the subsequent measurement. Similar results are obtained after the X_2 operation with the input states of $|0\rangle$ and $|1\rangle$. The final output results of all the measurements ranged from WWW ($y_1 \neq z_1$, $y_2 \neq z_2$, and $y_3 \neq z_3$) to RRR ($y_1 = z_1$, $y_2 = z_2$, and $y_3 = z_3$). If there is advice, the correct results would be obtained at the corresponding position and subsequent measurements for the quantum case. However, for the case with a single classical bit, the advice is helpful only in the initial position. We then calculate the average scores for each case according to Eq. (1), which is shown in Fig. 4(b). The maximal average score is achieved for the quantum case with the advice before the y_1 measurement. In the classical case, when the number of bits is less than k, y_1, y_2, and y_3 are unrelated and the same as the randomly generated case. Consequently, only the advice provided at the initial state can increase the average score. For all the situations, the average scores with a single qubit are larger than those with a classical bit.

IV. DISCUSSION AND CONCLUSION

We design a powerful quantum online stream algorithm suitable for dealing with huge online input data. The algorithm is implemented on a single spin defect in SiC at room temperature. The input data are converted to the corresponding rotations of the single spin qubit. The final output results are related to the intermediate results when the qubit are employed. Meanwhile, the results are completely random when the classical bit is employed. The algorithm performance depended on the position of the advice both for the quantum and classical cases. However, the algorithm with a single qubit always perform better than the classical one with a single bit. In this work, the length of the stream data is set to 40. The length can be greatly extended by prolonging the spin coherence time and the dephasing time, which can be realized by improving the sample preparation [24], applying the spin-locking technology [25] and encoding in the decoherence protected subspace [26]. We also provide a method to simplify the qubit rotation with a relatively large k in Appendix C. Our work demonstrates another example of the algorithm showing the quantum advantage, which would be useful in investigating complex online problems. This method can be extended to deal with a more complex problem with mod m and $m > 2$ (see Appendix D for more details). Considering the mature fabrication abilities on the technical material, the defect spins in SiC would be useful for future scalable quantum communication and computation. We consider only classical input data herein. The online stream algorithm with the quantum input data will also be of great interest. For example, quantum metrology [27–30] providing a much better precision than its classical counterpart, can be treated as quantum operations on a series of input entangled states. One natural and promising direction is to implement quantum metrology as the decoding part of quantum online algorithms. The memory effect of quantum metrology [31] can also be utilized if a multiqubit setup is adopted.

ACKNOWLEDGMENTS

This work is supported by the National Key Research and Development Program of China (Grant No. 2016YFA0302700), the National Natural Science Foundation of China (Grants No. U19A2075, No. 61725504, No. 11774335, No. 11821404, No. 61905233, and No. 11975221), the Key Research Program of Frontier Sciences, CAS (Grant No. QYZDY-SSW-SLH003), Science Foundation of the CAS (ZDRW-XH-2019-1), Anhui Initiative in Quantum Information Technologies (AHY060300 and AHY020100), the National Postdoctoral Program for Innovative Talents (Grant No. BX20200326), the Fundamental Research Funds for the Central Universities (Grants No. WK2030380017 and No. WK2470000026), the ERC (Consolidator Grant No. 683107/TempoQ) and the Alexander von Humboldt Foundation. This work is partially carried out at the USTC centre for Micro and Nanoscale Research and Fabrication.

APPENDIX A: ESTIMATION OF QUANTUM GATE FIDELITIES

When a qubit rotates along the x axis, the corresponding Hamiltonian in the rotating frame can be written as [32]

$$H = 2\pi\delta_0 S_z + 2\pi(f_1 + \delta_1)S_x, \tag{A1}$$

where S_x and S_z are the rotation matrices in the Bloch sphere along the x axis and z axis, respectively, f_1 represents the frequency of Rabi oscillation, δ_0 and δ_1 are the distributions of surrounding environmental noises. We assume that δ_0 follows the Gaussian distribution $G(\delta_0) = \exp(-\delta_0^2/2\beta^2)/(\sqrt{2\pi}\beta)$ and δ_1 follows the Lorentzian distribution $L(\delta_1) = \gamma/\pi(\gamma^2 + \delta_1^2)$, where β is the full width at half maximum of the Gaussian curve and γ is the one of Lorentz curve. The decay time of Rabi oscillation T_2' and the dephasing time T_2^* can be obtained from Eq. (2), which are read as $1/2\pi\gamma$ and $1/\sqrt{2}\pi\beta$, respectively. In Figs. 3(a) and 3(b) in the main text, γ is fitted to be 0.017 ± 0.001 MHz and β is fitted to be 0.158 ± 0.004 MHz.

In the experiment, three kinds of gates are implemented, i.e., the NOT gate, 0 gate, and 1 gate. The corresponding rotation matrices can be written as

$$U_{\mathrm{NOT}} = \exp\{-i[2\pi\delta_0 S_z + 2\pi(f_1 + \delta_1)S_x]t_\pi\}, \tag{A2}$$

$$U_0 = \exp[-i(2\pi\delta_0 S_z)t_0], \tag{A3}$$

$$U_1 = \exp\{-i[2\pi\delta_0 S_z + 2\pi(f_1 + \delta_1)S_x]t_1\}, \tag{A4}$$

where t_π is the time to apply a π pulse for the NOT gate, t_0 is the applied time of idle pulse to realize the 0 gate and t_1 is the applied time of microwave pulse to realize the 1 gate. In the experiment, t_0, t_1 are set to be 10 ns $t_\pi/2^k$, respectively.

The average fidelity of quantum gates in a solid-state spin system can be written as [33]

$$\overline{F} = \frac{1}{2} + \frac{1}{12}\sum_{j=x,y,z} \mathrm{Tr}(U_I\sigma_j U_I^\dagger U_P\sigma_j U_P^\dagger), \tag{A5}$$

where σ_j are the Pauli matrices. U_I and U_P are the ideal and practical operation matrices, respectively. Ideally, the matrices of NOT gate, 0 gate, and 1 gate can be written as $U_{\mathrm{NOT}_I} = \exp[-i(2\pi f_1 S_x)t_\pi]$, $U_{0_I} = \exp(-iIt_0)$, and $U_{1_I} = \exp[-i(2\pi f_1 S_x)t_1]$. For the NOT gate, we apply it only to the states $|0\rangle$ and $|1\rangle$. We obtain the fidelity of $F_{\mathrm{NOT}} = 0.928 \pm 0.017$ with $t_\pi = 0.704 \pm 0.001$ μs. By reducing t_π, F_{NOT} can be increased. According to Eq. (6), the fidelity of the 0 gate also can be calculated theoretically as $\overline{F}_0 = 0.999\,98 \pm 0.000\,01$ with the length of idle pulse

TABLE I. Random data streams in the experiment, where X_1, X_2, and X_3 are the generated random data streams, z_1, z_2, and z_3 are the corresponding theoretical predictions, 1 corresponds to a $\pi/2^{(k+1)}$ pulse and 0 corresponds to an idle pulse in experiment.

Serial number	k	X_1	X_2	X_3	z_1	z_2	z_3
1	4	11000001010110100001	11111111111001011111	01110101101111110101	1	0	0
		10000000100011111100	01011011111101111101	11111101111111111110			
2	4	10111000000010110011	10101111101101101111	01010010000010000100	0	1	1
		00001001011100010001	11110111111011110111	10101110010001111001			
3	4	11101111111111111110	00100101110010100001	00100001100010010000	0	0	1
		11111111010001001111	00010101011011000010	11001101000111100101			
4	2	111111101	100110100	011001010	0	0	1

$t_0 = 10 \pm 2$ ns. While for the 1 gate, the fidelity is related to k, which becomes $\overline{F}_1 = \frac{1}{2} + \frac{1}{6}\exp\{-[(\pi\beta T_\pi)^2/2^{2k+3}]\} + \frac{1}{6}\exp[-(\pi\gamma T_\pi/2^{k+2})] + \frac{1}{6}\exp\{-[(\pi\beta T_\pi)^2/2^{2k+3}] - (\pi\gamma T_\pi/2^{k+2})\}$.

When applying l identical gates sequentially, the average fidelity can be written as [32]

$$\overline{F} = 1/2 + 1/2(2F_i - 1)^l, \tag{A6}$$

where F_i is the single-shot average fidelity.

APPENDIX B: DETAILED RANDOM DATA STREAMS IN THE EXPERIMENT

The random sequence used in the main text is shown in Table I.

APPENDIX C: SIMPLIFICATION OF QUBIT ROTATION ANGLE $\pi/2^k$

In the quantum streaming algorithm, when k is relatively large, the precision of the rotation angle $\pi/2^k$ should be very high. Here, we propose a method to simplify the process. The number of 1 in the stream is supposed to be $v \times 2^k$. We introduce two integers, i.e., p and g, which satisfies $k = p + g$. For the smallest g, which satisfies

$$\begin{aligned} (v \times 2^p) \ \ \mathbf{mod} \ \ m \ &\equiv \ v \ \ \mathbf{mod} \ \ m, \\ (v \times (2^p - 1)) \ \ \mathbf{mod} \ \ m \ &\equiv \ 0, \\ (2^p - 1) \ \ \mathbf{mod} \ \ m \ &\equiv \ 0, \end{aligned} \tag{C1}$$

where m is a positive integer, we can reduce the rotation angle to $\pi/2^g$.

For a more general case, we assume that q and f satisfy $2^k = q \times f$, that is, $\text{no.}_1(X_i) = v(X_i) \times q \times f$. For the smallest f, which satisfies

$$\begin{aligned} (v * q) \ \ \mathbf{mod} \ \ m \ &\equiv \ v \ \ \mathbf{mod} \ \ m, \\ [v * (q-1)] \ \ \mathbf{mod} \ \ m \ &\equiv \ 0, \\ (q-1) \ \ \mathbf{mod} \ \ m \ &\equiv \ 0, \end{aligned} \tag{C2}$$

we can reduce the rotation angle to π/f.

APPENDIX D: THE GENERAL SCHEME FOR MOD m WITH MULTIPLE QUBITS

We extend the quantum stream algorithm to the case of calculating $v(X_i)$ **mod** m ($m > 2$), which should be implemented with high-dimensional systems or multiple qubits. The number of 1's in X_i is assumed to be in the form of $\text{no.}_1(X_i) = v(X_i) \times 2^k$. For simplicity, we consider the case where $m = 2^n$. The initial state is prepared to be $|0\rangle^{\otimes n}$. When the algorithm reads 1, the first qubit is rotated by an angle of $\alpha = \pi/2^k$. While for the nth qubit, the rotation angle is $\alpha/2^{n-1}$. After no.(1) rotations, the possible state for the nth qubit is one of the states $\{\cos(\pi/2^n \times 0)|0\rangle + \sin(\pi/2^n \times 0)|1\rangle, \cos(\pi/2^n \times 1)|0\rangle + \sin(\pi/2^n \times 1)|1\rangle, \ldots, \cos[\pi/2^n \times (2^{(n-1)} - 1)]|0\rangle + \sin[\pi/2^n \times (2^{(n-1)} - 1)]|1\rangle\}$.

The measurement basis of the nth qubit depends on measurement result of the $(n-1)$th qubit. For example, if the measurement result of the lth qubit is $\cos(\pi/2^l \times h)|0\rangle + \sin(\pi/2^l \times h)|1\rangle$, then the $(l+1)$th qubit measurement basis is $\{\cos(\pi/2^{l+1} \times h)|0\rangle + \sin(\pi/2^{l+1} \times h)|1\rangle, \cos[\pi/2^{l+1} \times (2^l + h)]|0\rangle + \sin[\pi/2^{l+1} \times (2^l + h)]|1\rangle\}$. If the measurement result of the nth qubit is $\cos(\pi/2^n \times s)|0\rangle + \sin(\pi/2^n \times s)|1\rangle$, then v **mod** $2^n = s$.

Considering the case with advice, the usage of entangled states would greatly reduce the transmitted qubits. Similar to implement the dense coding protocol [34], only one qubit transmission is needed when the advice information is encoded in a two-qubit EPR state [3]. While two classical bits are required to reveal the full advice information. Similarly, if there is advice information needed to encode in k qubits, only $k/2$ qubits are needed to transmit.

[1] A. Mehta, A. Saberi, U. Vazirani, and V. Vazirani, Adwords and generalized online matching, ACM **54**, 22 (2007).

[2] A. Mehta, Online matching and ad allocation, Theory Comput. Sci. **8**, 265 (2012).

[3] K. Khadiev, A. Khadieva, and I. Mannapov, Quantum online algorithms with respect to space and advice complexity, Lobachevkii J. Math. **39**, 1377 (2018).

[4] S. Albers, in *Interactive Computation*, edited by D. Goldin, S. A. Wegner, and P. Smolka, (Springer, Berlin, Heidelberg, 2006), p. 143.

[5] H. Fujiwara and K. Iwama, Average-case competitive analyses for ski-rental problems, Algorithmica **42**, 95 (2005).

[6] H. Fujiwara and K. Iwama, in *International Symposium on Algorithms and Computation* (Springer, Berlin, Heidelberg, 2002), p. 476.

[7] I. Mitliagkas, C. Caramanis, and P. Jain, in *Proceedings of the 26th International Conference on Neural Information Processing Systems* (Curran Associates Inc., New York, 2013), Vol. 2, p. 2886.

[8] R. Vaze, in *Proceedings of the 32nd IEEE International Conference on Computer Communications (INFOCOM),* (IEEE, Turin, Italy, 2013), p. 1115.

[9] S. Miyazaki, On the advice complexity of online bipartite matching and online stable marriage, Process. Lett. **114**, 714 (2014).

[10] H.-J. Böckenhauer, S. Geulen, D. Komm, and W. Unger, *Constructing Randomized Online Algorithms from Algorithms With Advice* (Technical report, ETH Zurich, 2015).

[11] P. W. Shor, in *Proceedings 35th Annunual Symposium on Foundations of Computer Science* (IEEE Computer Society Press, Santa Fe, New Mexico, 1994), p. 124.

[12] L. K. Grover, Quantum Mechanics Helps in Searching for a Needle in a Haystack, Phys. Rev. Lett. **79**, 325 (1997).

[13] F. L. Gall, Exponential separation of quantum and classical online space complexity, Theory Comput. Syst. **45**, 188 (2009).

[14] A. Cabello, M. Gu, O. Gühne, and Z. P. Xu, Optimal Classical Simulation of State-Independent Quantum Contextuality, Phys. Rev. Lett. **120**, 130401 (2017).

[15] A. Karanjai, J. J. Wallman, and S. D. Bartlett, Contextuality bounds the efficiency of classical simulation of quantum processes, ArXiv:1802.07744 (2018).

[16] M. Nagy and S. G. Akl, Quantum computing: Beyond the limits of conventional computation, Int. J. Parallel Emergent Distrib. Syst. **22**, 123 (2007).

[17] N. T. Son, C. P. Anderson, A. Bourassa, K. C. Miao, C. Babin, M. Widmann, M. Niethammer, J. Ul Hassan, N. Morioka, I. G. Ivanov, and F. Kaiser, Developing silicon carbide for quantum spintronics, Appl. Phys. Lett. **116**, 190501 (2020).

[18] D. J. Christle, P. V. Klimov, F. Charles, K. Szász, V. Ivády, V. Jokubavicius, J. U. Hassan, M. Syväjärvi, W. F. Koehl, T. Ohshima, and N. T. Son, Isolated Spin Qubits in SiC with a High-Fidelity Infrared Spin-To-Photon Interface, Phys. Rev. X **7**, 021046 (2017).

[19] W. F. Koehl, B. B. Buckley, F. J. Heremans, G. Calusine, and D. D. Awschalom, Room temperature coherent control of defect spin qubits in silicon carbide, Nature **479**, 84 (2011).

[20] F.-F. Yan, J.-F. Wang, Q. Li, Z. D. Cheng, J. M. Cui, W. Z. Liu, J. S. Xu, C. F. Li, and G. C. Guo, Coherent control of defect spins in silicon carbide above 550 K, Rev. Appl. **10**, 044042 (2018).

[21] A. L. Falk, B. B. Buckley, G. Calusine, W. F. Koehl, V. V. Dobrovitski, A. Politi, C. A. Zorman, P. X.-L. Feng, and D. D. Awschalom, Polytype control of spin qubits in silicon carbide, Nat. Commun. **4**, 1819 (2013).

[22] J.-F. Wang, Y. Zhou, X. M. Zhang, F. Liu, Y. Li, K. Li, Z. Liu, G. Wang, and W. Gao, Efficient Generation of an Array of Single Silicon-Vacancy Defects in Silicon Carbide, Phys. Rev. Appl. **7**, 064021 (2017).

[23] Q. Li, J.-F. Wang, F.-F. Yan, J. Y. Zhou, H. F. Wang, H. Liu, L. P. Guo, X. Zhou, A. Gali, Z. H. Liu, and Z. Q. Wang, Room temperature coherent manipulation of single-spin qubits in silicon carbide with high readout contrast, Nat. Sci. Rev. (2021).

[24] A. Bourassa, C. P. Anderson, K. C. Miao, M. Onizhuk, H. Ma, A. L. Crook, H. Abe, J. Ul-Hassan, T. Ohshima, N. T. Son, and G. Galli, Entanglement and control of single quantum memories in isotopically engineered silicon carbide, Nat. Mater. **19**, 1319 (2020).

[25] D. Simin, H. Kraus, A. Sperlich, T. Ohshima, G. V. Astakhov, and V. Dyakonov, Locking of electron spin coherence above 20 ms in natural silicon carbide, Phys. Rev. B **95**, 161201(R) (2017).

[26] K. C. Miao, J. P. Blanton, C. P. Anderson, A. Bourassa, A. L. Crook, G. Wolfowicz, H. Abe, G. Ohshima, and D. D. Awschalom, Universal coherence protection in a solid-state spin qubit, Science **369**, 1493 (2020).

[27] G. Toth and I. Apellaniz, Quantum metrology from a quantum information science perspective, J. Phys. A: Math. Theor. **47**, 424006 (2014).

[28] V. Giovannetti, S. Lloyd, and L. Maccone, Quantum-enhanced measurements: Beating the standard quantum limit, Science **306**, 1330 (2004).

[29] V. Giovannetti, S. Lloyd, and L. Maccone, Quantum Metrology, Phys. Rev. Lett. **96**, 010401 (2006).

[30] R. Demkowicz-Dobrzański, J. Kołodyński, and M. Guţă, The elusive Heisenberg limit in quantum-enhanced metrology, Nat. Commun. **3**, 1063 (2012).

[31] Y. Yang, Memory Effects in Quantum Metrology, Phys. Rev. Lett. **123**, 110501 (2019).

[32] X. Rong, J. P. Geng, F. Z. Shi, Y. Liu, K. Xu, W. Ma, F. Kong, Z. Jiang, Y. Wu, and J. Du, Experimental fault-tolerant universal quantum gates with solid-state spins under ambient conditions, Nat. Commun. **6**, 8748 (2015).

[33] M. D. Bowdrey, D. K. L. Oi, A. J. Short, K. Banaszek, and J. A. Jones, Fidelity of single qubit maps, Phys. Lett. A **294**, 258 (2002).

[34] C. H. Bennett and S. J. Wiesner, Communication via One- and Two-Particle Operators on Einstein-Podolsky-Rosen States, Phys. Rev. Lett. **69**, 2881 (1992).